Bioorganic & Medicinal Chemistry Letters 25 (2015) 5555–5560

Contents lists available at ScienceDirect

Bioorganic & Medicinal Chemistry Letters

journal homepage: www.elsevier.com/locate/bmcl

Discovery of 1*H*-pyrazolo[3,4-*b*]pyridines as potent dual orexin receptor antagonists (DORAs)

Dirk Behnke [a,*], Simona Cotesta [a], Samuel Hintermann [a], Markus Fendt [b], Christine E. Gee [b], Laura H. Jacobson [b,f], Grit Laue [c], Arndt Meyer [a], Trixie Wagner [a], Sangamesh Badiger [d], Vinod Chaudhari [d], Murali Chebrolu [d], Chetan Pandit [d], Daniel Hoyer [b,e,f], Claudia Betschart [a]

[a] *Global Discovery Chemistry, Novartis Institutes for BioMedical Research, WKL-136.3.26, CH-4002 Basel, Switzerland*
[b] *Neuroscience, Novartis Institutes for BioMedical Research, CH-4002 Basel, Switzerland*
[c] *Metabolism and Pharmacokinetics, Novartis Institutes for BioMedical Research, CH-4002 Basel, Switzerland*
[d] *Medicinal Chemistry, Aurigene Discovery Technologies Limited, 39-40, KIADB Industrial Area, Phase II, Electronic City, Hosur Road, Bangalore 560100, India*
[e] *School of Biomedical Sciences, Faculty of Medicine, Dentistry and Health Sciences, The University of Melbourne, Parkville, Victoria 3010, Australia*
[f] *The Florey Institute of Neuroscience and Mental Health, Parkville Campus, Kenneth Myer Building at Genetics Lane, on Royal Parade, University of Melbourne, Parkville, 3010, Australia*

ARTICLE INFO

Article history:
Received 13 August 2015
Revised 16 October 2015
Accepted 18 October 2015
Available online 19 October 2015

Keywords:
Orexin
GPCRs
Insomnia
Antagonists

ABSTRACT

Compound *rac*-**1** was identified by high throughput screening. Here we report SAR studies and MedChem optimization towards the highly potent dual orexin receptor antagonists (*S*)-**2** and (*S*)-**3**. Furthermore, strategies to overcome the suboptimal physicochemical properties are highlighted and the pharmacokinetic profiles of representative compounds is presented.

The orexin receptor 1 (OX_1R) and the orexin receptor 2 (OX_2R) are two G-protein coupled receptors widely expressed in the brain. The two endogenous neuropeptide agonists, orexin-A and orexin-B (also known as hypocretin 1 and hypocretin 2), are selectively expressed in a small cluster of neurons in the lateral hypothalamus.[1,2] Activation of the orexin system by these peptides promotes wakefulness in animals and humans.[3–5] Consequently, the discovery of OX_1R and OX_2R antagonists has become a major focus of research for the treatment of (primary) insomnia over the past years. Positive clinical proof of concept (PoC) were achieved with Merck's dual $OX_{1,2}R$ antagonists (DORAs) suvorexant (MK-4305) and filorexant (MK-6096), Actelion's almorexant (ACT-078573) and Glaxo SmithKline's SB-649868 (Fig. 1).[6–11] In 2014 suvorexant (tradename BELSOMRA®) was approved in the U.S. and Japan as the first orexin antagonist for the treatment of primary insomnia.

In 2007, a drug discovery project was initiated at Novartis with the aim to identify dual orexin receptor antagonists. Here we report the discovery, SAR and optimization of a series of novel substituted 1*H*-pyrazolo[3,4-*b*]pyridines as potent DORAs.

rac-**1** was identified as a promising hit in a high throughput screen (HTS) of the Novartis compound collection. It showed dual potency on both orexin receptors in the cell-based functional Calcium accumulation assay (as measured by FLIPR, fluorometric imaging plate reader).[12] Receptor binding was used as secondary screen to confirm that *rac*-**1** binds with similar potency to both orexin receptors (Fig. 2).[13] The series was considered a good starting point for further optimization.

The initial SAR studies focused mainly on the amide motif of the molecule exploring the influence of modifications on potency and selectivity for both the hOX_1R and hOX_2R. A diverse set of derivatives with differently substituted aryl/heteroaryl substituents was synthesized (Table 1). The most promising results were obtained with chiral benzylic aryl/heteroaryl amine substituents. The *para* methoxy derivative *rac*-**2** and the pyrazole compound *rac*-**3** were found to be most potent on the hOX_2R with *rac*-**2** showing a slight trend for hOX_2R selectivity. Compound *rac*-**2** containing a *para*-methoxy substituent were more potent on both orexin receptors than *rac*-**4** with a methoxy substituent in *ortho* position. A comparison of *rac*-**2** with the *meta* methoxy substituted compound *rac*-**5** showed equivalent affinity for the hOX_1R and 10-fold improved affinity for the hOX_2R. Compounds with electron poor heteroaryls

* Corresponding author. Tel.: +41 61 696 29 59; fax: +41 61 696 23 30.
E-mail address: dirk.behnke@novartis.com (D. Behnke).

http://dx.doi.org/10.1016/j.bmcl.2015.10.055
0960-894X/

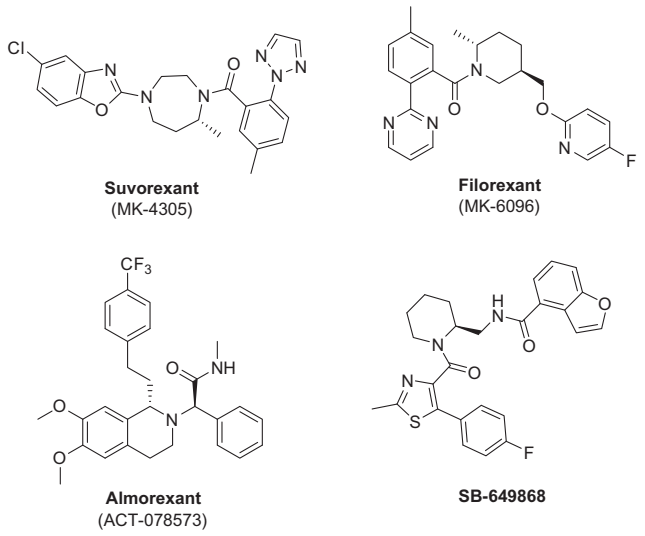

Figure 1. DORAs that have achieved positive clinical proof of concept.

such as the pyridine analogs *rac*-**6** and *rac*-**7** were less favored. The highly potent hOX_2R antagonists *rac*-**2** and *rac*-**3** were subjected to chiral separation yielding compounds (*S*)-**2**/(*R*)-**2** and (*S*)-**3**/(*R*)-**3**. In parallel, compounds (*S*)-**2** and (*R*)-**2** were synthesized using commercially available enantiomerically pure (*S*) and (*R*)-1-(4-methoxyphenyl)ethanamine. Compound (*S*)-**2** was found to be the active enantiomer whereas compound (*R*)-**2** lost activity on both orexin receptors. Likely, the (*R*)-configuration of the methyl group forced the compounds into a conformation that is unfavorable for binding to the orexin receptors. Compound **8** was more than one order of magnitude less potent than (*S*)-**2** on both receptors, further supporting the importance of the properly configured methyl group. By analogy, the absolute configuration in compounds (*S*)-**3** and (*R*)-**3** obtained by chiral separation of the enantiomers were assigned based on their potency on hOX_1R and hOX_2R. Removal of the core N–Me in (*S*)-**9** gave compound (*S*)-**10** which was equipotent on both hOX_1R and hOX_2R suggesting that the N–H cannot engage in a hydrogen bond interaction with the orexin receptors. Interestingly, replacing the ether oxygen in the side chain by NH was detrimental for potency on the hOX_2R (10-fold loss) whereas for hOX_1R only a marginal shift was observed, resulting in an hOX_1R preferring antagonist (see compound (*S*)-**11** vs (*S*)-**9**). Methylation of the pyrazole of (*S*)-**3** resulted in compound (*S*)-**12** where dual potency could be maintained in a desired range and an active transport mechanism as the most likely reason for unfavorable brain penetration of (*S*)-**3** was significantly suppressed (see also paragraph in vivo characterization and PK properties). More drastic changes at the core to reduce lipophilicity as exemplified by compound (*S*)-**13** led to loss of potency on both receptors compared to (*S*)-**2** and (*S*)-**3**.

The synthesis of compound (*S*)-**3** as a representative example for this class is shown in Scheme 1.[14] Ester condensation of methyl benzoate **14** with acetonitrile using sodium hydride as base yielded the α-cyano ketone **15**. Ring closure to the corresponding amino pyrazole **16** was achieved with methyl hydrazine in methanol in moderate yield. For derivatives with other substituents at the 3-position of the pyrazolopyridine core, the sequence was started with the corresponding aryl/heteroaryl ester analogs of **14**. Microwave-assisted reaction of **16** with ethyl 4,4,4-trifluoro-3-oxobutanoate in acetic acid gave compound **17**. The alkylation of **17** with ethyl 2-bromoacetate using sodium hydride in DMF selectively gave the O-alkylation product **18**. Compound **18** was subsequently subjected to ester hydrolysis yielding compound **19**, which was the precursor for the last amide coupling step. If available, enantiomeric pure amines with known absolute configuration were used for the amide formation, otherwise chiral separations were performed after the final step (e.g., for compound (*S*)-**3**). In such cases the absolute configuration was assigned based on the biological activity.

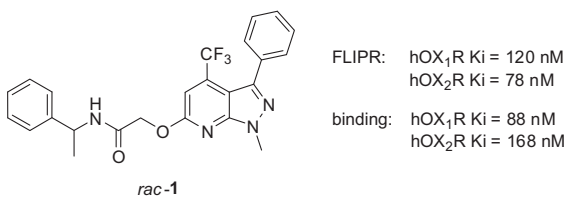

Figure 2.

The overall in vitro profiles of compounds (*S*)-**2** and (*S*)-**3** are illustrated in Table 2. Both compounds are potent dual orexin receptor antagonists as measured in the functional Calcium as well as radioligand binding assays. Although high potencies were achieved, the physicochemical properties were less than optimal. Both (*S*)-**2** and (*S*)-**3** have high lipophilicity (HT-log *P* of 4.60 and 4.20) resulting in low solubility measured in a high throughput format at pH 6.8. Permeation measured in a PAMPA assay was high, indicting they are class II compounds based on the Biopharmaceutics Classification System (BCS).[16] The CYP inhibition profile of compound (*S*)-**3** was better than that of compound (*S*)-**2**, for which CYP3A4 and CYP2C9 were inhibited with IC_{50}'s of 8 and 5 μM, respectively. Both compounds had high in vitro clearances in rat, human and mouse liver microsomes and high plasma protein binding, leading to plasma free-fractions of less than 1% in mouse. Compounds (*S*)-**2** and (*S*)-**3** had no hERG flag and an excellent in vitro selectivity and off-target profile.

With highly potent compounds in hand, in vivo characterization was initiated. The blood pharmacokinetic (PK) and brain penetration properties of compounds (*S*)-**2** and (*S*)-**3** were tested in the mouse (Table 3) in a cassette dosing setup; i.e., five experimental compounds and a reference compound were administered together intravenously at 1 mg/kg and per os at 3 mg/kg. Compound (*S*)-**2** exhibited a medium blood clearance, a moderate volume of distribution and a relatively short terminal half-life. The absolute oral bioavailability was very low (*F* = 3%) but the brain/blood concentration ratio (br/bl = 1.15) indicated favorable brain penetration. For compound (*S*)-**3** the blood clearance was low and, in contrast to compound (*S*)-**2**, the oral bioavailability was moderate (*F* = 21%), and as such the AUC of (*S*)-**3** after oral dosing was higher than that of compound (*S*)-**2**. The brain/blood concentration ratio of 0.02 for compound (*S*)-**3** indicated a very low brain penetration (if at all). A possible reason might be P-glycoprotein (P-gp) activity as measured in the MDCK assay. Compound (*S*)-**3** showed a BA/AB efflux ratio of 23 in human MDCK cells stably expressing MDR1 and is therefore a human P-glycoprotein substrate, which is likely to also be the case in mice. The efflux of compound (*S*)-**3** could be considerably reduced for compound (*S*)-**12** (Table 1) with an efflux ratio of 3.

Compound (*S*)-**3** showed a limited correlation between in vitro and in vivo clearance (high in vitro, low in vivo). A potential hypothesis for this disconnect is a restrictive binding to plasma proteins (very high plasma protein binding of >99% in mice), which might protect the compound from metabolism in vivo.

The next round of optimization aimed to improve the physicochemical properties, in particular reducing lipophilicity and improving solubility, with the goal of generating compounds with improved PK properties. In order to achieve this, we initially focused on the optimization and profiling of compound (*S*)-**9**.

Table 1
Amide moiety SAR

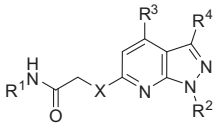

Compd	R^1	R^2	R^3	R^4	X	hOX_1R Calcium K_i (nM)	hOX_2R Calcium K_i (nM)	Ratio hOX_1R/hOX_2R
rac-**1**		Me	CF_3	Ph	O	120	78	1.54
rac-**2**	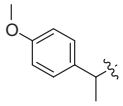	Me	CF_3	Ph	O	29	2	14.50
rac-**3**	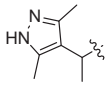	Me	CF_3	Ph	O	4	3	1.33
rac-**4**	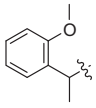	Me	CF_3	Ph	O	274	158	1.73
rac-**5**	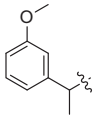	Me	CF_3	Ph	O	20	26	0.77
rac-**6**		Me	CF_3	Ph	O	2667	No inh.	—
rac-**7**	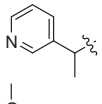	Me	CF_3	Ph	O	970	582	1.67
(*S*)-**2**	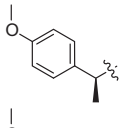	Me	CF_3	Ph	O	14	2	7.00
(*R*)-**2**	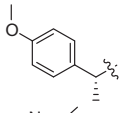	Me	CF_3	Ph	O	2287	949	2.41
(*S*)-**3**	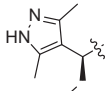	Me	CF_3	Ph	O	5	2	2.50
(*R*)-**3**	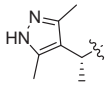	Me	CF_3	Ph	O	>4000	>2000	—
8	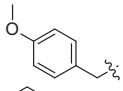	Me	CF_3	Ph	O	800	83	9.64
(*S*)-**9**		Me	CF_3	Ph	O	175	108	1.62
(*S*)-**10**		H	CF_3	Ph	O	200	43	4.65
(*S*)-**11**		Me	CF_3	Ph	NH	357	1135	0.31
(*S*)-**12**	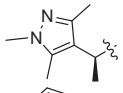	Me	CF_3	Ph	O	7	10	0.70
(*S*)-**13**	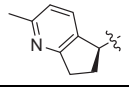	Me	CH_3	cyclo-propyl	O	109	22	4.95

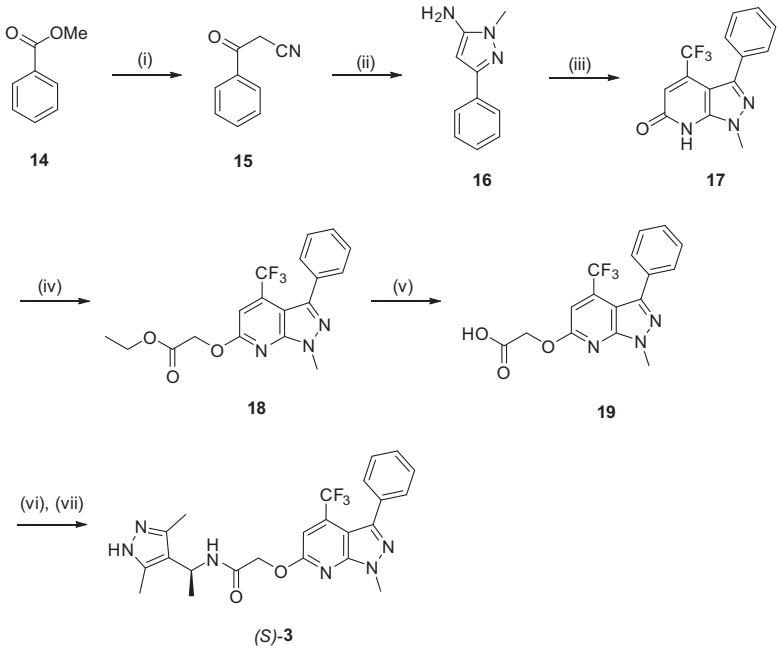

Scheme 1. Reagents and conditions: (i) NaH, DMSO, MeCN, rt, 66%; (ii) $MeNHNH_2$, MeOH, 110 °C, 57%; (iii) CF_3COCH_2COOEt, AcOH, 150 °C, microwave, 64%; (iv) $BrCH_2COOEt$, NaH, DMF, rt, 77%; (v) aq LiOH, EtOH/THF, rt, 92%; (vi) (*rac*)-**1**-(3,5-dimethyl-1*H*-pyrazol-4-yl)ethanamine, HOBt, DIC, DMF, 80 °C; (vii) chiral separation on HPLC, 23% (2 steps).

Table 2
In vitro profile of compounds (*S*)-**2** and (*S*)-**3**

Property	(*S*)-**2**	(*S*)-**3**
hOX_1R Calcium K_i (nM)	14	5
hOX_2R Calcium K_i (nM)	2	2
hOX_1R binding K_i (nM)	8	3
hOX_2R binding K_i (nM)	4	8
HT-log *P*[15]	4.60	4.20
HT-eq. sol (pH 6.8) (mM)	<0.004	<0.004
Log PAMPA	−4	−4.1
MDCK[a] BA/AB efflux ratio	1	23
CYP inh. 3A4/2D6/2C9 IC_{50} (μM)	8/>20/5	>20/>20/>20
Cl_{int} (μL/min * mg) RLM/HLM/MLM	147/190/478	603/433/330
PPB (%) h/m	>99/>99	96/>99
hERG IC_{50} (μM) binding/QPatch	>30/n.d.	>30/>30
Number off-targets with IC_{50} < 1 μM	0/108[b]	0/112[b]

[a] PgP-mediated transport of compounds was tested in a medium-throughput assay in 24-well plates using MDCK cells stably expressing MDR1 (Madin–Darby Canine Kidney cells retrovirally transduced with the human multidrug resistance gene 1; P-glycoprotein PgP).
[b] Compounds were tested against a number of safety relevant off-targets (108 for (*S*)-**2**) and 112 for (*S*)-**3**) including receptors, proteases, kinases etc.; no off-target was affected by (*S*)-**2** and (*S*)-**3** at IC_{50}'s below 1 μM.

Table 3
Mouse in vivo PK data of selected compounds[b]

Compd	Intravenous dose 1 mg/kg[c]			Oral dose 3 mg/kg[d]			
	Cl_{bl} (mL min^{-1} kg^{-1})	*V*ss (L/kg)	$t_{1/2term}$ (h)	$C_{max,bl}$ d.n. (nM)	AUC_{bl}[e] d.n. (nM * h)	*F*[f] (%)	[br]/[bl] at 1 h p.d. ± SD[g]
(*S*)-**2**	65	2.0	1.1	4	17	3	1.15 ± 0.24
(*S*)-**3**	20	0.5	0.5	300	371	21	0.02 ± 0.01
(*S*)-**13**	66	0.4	0.3	115	106	16	0.13 ± 0.02

[b] The absorption and disposition parameters were estimated by a non-compartmental analysis of the mean blood concentration ($n = 3$) versus time profile after oral and intravenous administration; dosing was in a cassette of 6 compounds.
[c] Dosed as a solution in NMP/blank plasma (10:90, v/v).
[d] Dosed as a suspension in carboxymethylcellulose 0.5% w/v in water/Tween 80 (99.5%/0.5%, v/v).
[e] AUC was extrapolated to infinity.
[f] Absolute oral bioavailability was calculated by dividing the dose-normalized AUC after oral and intravenous dosing assuming linear pharmacokinetics between these 2 doses.
[g] Mean brain/blood concentration ratio from $n = 3$; d.n. = dose-normalized, i.e., calculated to a dose of 1 mg * kg^{-1}.

Table 4
Compounds with improved physicochemical properties

Compd	Structure	hOX$_1$R Calcium K_i (nM)	hOX$_2$R Calcium K_i (nM)	HT-log *P*	HT-eq. sol (pH 6.8) (mM)
(*S*)-**20**	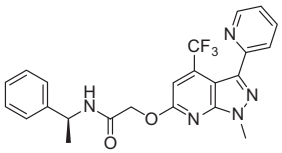	660	367	3.50	0.04
(*S*)-**21**	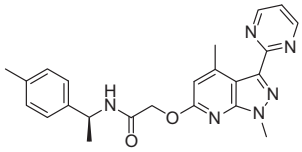	4	5	3.30	0.043
(*S*)-**22**	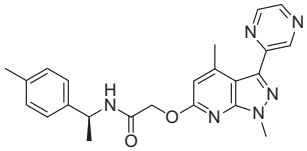	52	15	3.90	0.115
rac-**23**	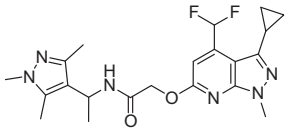	778	527	2.80	0.657
(*S*)-**24**	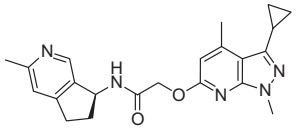	783	93	3.50	0.025
rac-**25**	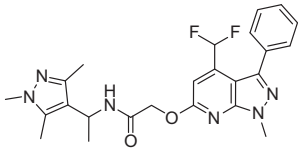	63	59	3.90	0.248

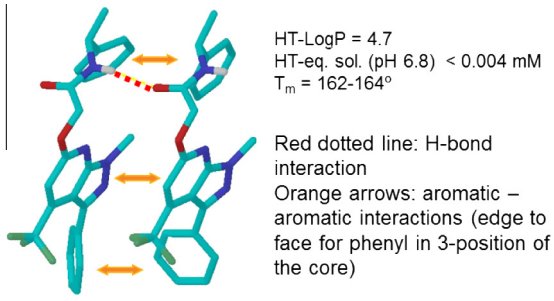

Figure 3. X-ray crystal interaction of compound (*S*)-**9**.

The in vitro biotransformation of compound (*S*)-**9** after incubation with mouse and human liver microsomes and the in vivo biotransformation in mouse revealed two major metabolic pathways: oxidation at the benzylic position of the amide part and oxidation at the phenyl ring in 3-position of the core (data of biotransformation studies not shown). Attempts to address the metabolic weak spot at the amide benzylic position by introducing non-aromatic moieties and by altering the length of the amide side chain were less successful. Compounds (*S*)-**20**, (*S*)-**21** and (*S*)-**22** (Table 4) were therefore designed to reduce the potential for oxidation at the phenyl ring by introducing electron poor aryls. These variations, in parallel, were beneficial for improving the log *P*. A small molecule X-ray analysis of compound (*S*)-**9**[17] shows an intermolecular hydrogen bond interaction between the amide carbonyl and the amide NH. In addition, strong intermolecular aromatic interactions are present (indicated by the arrows, Fig. 3). The core phenyl in 3-position is involved in 'edge to face' interactions. The low solubility of compound (*S*)-**9** is therefore the result of a combination of high crystal lattice energy (reflected by the melting point of 162–164 °C) and high lipophilicity (as shown by the HT-log *P* of 4.7). Unfortunately, attempts to reduce crystal lattice energy through interruption of the hydrogen bond by N-alkylation led to a loss in potency. Consequently, another strategy aimed at reducing stacking by adding non-aromatic moieties in the 3-position (see compounds *rac*-**23** and (*S*)-**24**). Results are shown in Table 4.

The comparison of the pyridyl compound (*S*)-**20** with (*S*)-**9** indicates a significantly reduced lipophilicity (HT-log *P* of 4.7 for (*S*)-**9** vs 3.50 for (*S*)-**20**) also resulting in improved solubility of 0.04 mM at pH 6.8. The potencies on both orexin receptors slightly decreased but could be restored by introducing a methyl group in the *para* position of the amide aryl. This substitution in combination with the pyrimidine substituent in 3-position resulted in the highly potent dual orexin receptor antagonist (*S*)-**21** with improved HT-log *P* of 3.30 and a solubility of 0.043 mM. The pyrazine analog (*S*)-**22** showed better solubility but was less potent on hOX$_1$R and hOX$_2$R. Replacement of the aromatic 3-substituent by a cyclopropyl group was partially successful at improving the solubility as shown for *rac*-**23** but this improvement often occurred at the expense of reduced potencies on hOX$_1$R and hOX$_2$R. A successful strategy to keep the potency in a desired range but reduce the lipophilicity was the modification of the CF_3 group by CH_3 and CHF_2 replacements. The most pronounced effect for lowering the

log *P* was achieved with the CHF_2 group and the lipophilicity usually decreased in the order $CF_3 > CH_3 > CHF_2$. Although the solubility could be improved for some compounds (see e.g., *rac*-**23** and *rac*-**25** in Table 4), this alteration did not translate in an improved in vitro metabolism. In general, all modifications mentioned above aimed at improving the physicochemical properties were not accompanied by reduced metabolism in vitro (Cl_{int} (μL/min * mg) in RLM: 924 for (*S*)-**20**, 660 for *rac*-**23**, 924 for (*S*)-**24**).

In conclusion, we have identified a series of 1*H*-pyrazolo[3,4-*b*] pyridines as potent orexin receptor antagonists by high throughput screening. Fast exploration of the SAR led to the dual orexin receptor antagonists (*S*)-**2** and (*S*)-**3** with high functional and binding potencies at hOX_1R and hOX_2R. Compounds (*S*)-**2** and (*S*)-**3** have shown a favorable off-target profile. PK studies revealed that the compounds have low to moderate clearance. Bioavailability and brain penetration were in a low to moderate range. The suboptimal physicochemical properties could be improved and compounds with improved solubility and lipophilicity features were identified. Overall, however, combining favorable in vitro pharmacology and in vivo PK properties remains challenging in this series. Compound (*S*)-**13** was found to be one of the best compromises between blood exposure and sufficient brain penetration to achieve brain exposure after oral dosing.

Acknowledgements

We thank J. Blanz, P. Ramstein, W. Gertsch and F. Blasco for the biotransformation study of compound **13**. Furthermore we thank Richard Felber, Sandrine Liverneaux, Andrea Hasler, Alfred Tanner, Thomas Gut, Marc Weibel, Fatma Limam, Marjorie Bourrel, Michael Wright for synthetic support, Dominique Monna, Edi Schuepbach and Daniel Langenegger for in vitro biological data, and Jürgen Wagner for management support and helpful discussions.

References and notes

1. Sakurai, T.; Amemiya, A.; Ishii, M.; Matsuzaki, I.; Chemelli, R. M.; Tanaka, H.; Williams, S. C.; Richardson, J. A.; Kozlowski, G. P.; Wilson, S.; Arch, J. R. S.; Buckingham, R. E.; Haynes, A. C.; Carr, S. A.; Annan, R. S.; Mcnulty, D. E.; Liu, W.-S.; Terrett, J. A.; Elshourbagy, N. A.; Bergsma, D. J.; Yanagisawa, M. *Cell* **1998**, *92*, 573.
2. De Lecea, L.; Kilduff, T. S.; Peyron, C.; Gao, X.-B.; Foye, P. E.; Danielson, P. E.; Fukuhara, C.; Battenberg, E. L. F.; Gautvik, V. T.; Bartlett, F. S., II; Frankel, W. N.; Van Den Pol, A. N.; Bloom, F. E.; Gautvik, K. M.; Sutcliffe, J. G. *Proc. Natl. Acad. Sci. U.S.A.* **1998**, *95*, 322.
3. Sakurai, T.; Ohno, K. *Front. Neuroendicrinol.* **2008**, *29*, 70.
4. Roecker, A. J.; Coleman, P. J. *Curr. Top. Med. Chem.* **2008**, *8*, 977.
5. Coleman, P. J.; Renger, J. J. *Expert Opin. Ther. Pat.* **2010**, *20*, 307.
6. Winrow, C. J.; Gotter, A. L.; Cox, C. D.; Doran, S. M.; Tannenbaum, P. L.; Breslin, M. J.; Garson, S. L.; Fox, S. V.; Harrell, C. M.; Stevens, J.; Reiss, D. R.; Cui, D.; Coleman, P. J.; Renger, J. J. *J. Neurogenet.* **2011**, *25*, 52.
7. Herring, W. J.; Snyder, E.; Budd, K.; Hutzelmann, J.; Snavely, D.; Liu, K.; Lines, C.; Roth, T.; Michelson, D. *Neurology* **2012**, *79*, 2265.
8. Brisbare-Roch, C.; Dingemanse, J.; Koberstein, R.; Hoever, P.; Aissaoui, H.; Flores, S.; Mueller, C.; Nayler, O.; van Gerven, J.; de Haas, S. L.; Hess, P.; Qiu, C.; Buchmann, S.; Scherz, M.; Weller, T.; Fischli, W.; Clozel, M.; Jenck, F. *Nat. Med.* **2007**, *13*, 150.
9. Hoyer, D.; Jacobson, L. H. *Neuropeptides* **2013**, *47*, 477.
10. Kuduk, S. D.; Winrow, C. J.; Coleman, P. J. *Annu. Rep. Med. Chem.* **2013**, *48*, 73.
11. Bettica, P.; Nucci, G.; Pyke, C.; Squassante, L.; Zamuner, S.; Ratti, E.; Gomeni, R.; Alexander, R. *J. Psychopharmacol.* **2012**, *26*, 1058.
12. Ca^{2+} accumulation (as measured by FLIPR, fluorometric imaging plate reader) was used as a functional readout of orexin receptor activity, for details see WO2011076744.
13. [^{125}I]-orexin A was used as radioligand in the binding assay, for details see: Badiger, S.; Behnke, D.; Betschart, C.; Chaudhari, V.; Chebrolu, M.; Cotesta, S.; Hintermann, S.; Meyer, A.; Pandit, C. Patent WO2011076744, 2011.
14. Experimental information: Detailed synthetic procedures are described. In Badiger, S.; Behnke, D.; Betschart, C.; Chaudhari, V.; Chebrolu, M.; Cotesta, S.; Hintermann, S.; Meyer, A.; Pandit, C. Patent WO2011076744, 2011.
15. Faller, B.; Grimm, H. P.; Loeuillet-Ritzler, F.; Arnold, S.; Briand, X. *J. Med. Chem.* **2005**, *48*, 2571.
16. Wu, C.-Y.; Benet, L. Z. *Pharm. Res.* **2005**, *22*, 11.
17. X-ray coordinates are deposited with the Cambridge Crystallographic Data Centre: CCDC deposition number 1429189.